Optimized Conformal Surface Registration with Shape-based Landmark Matching[*]

Lok Ming Lui[†], Sheshadri Thiruvenkadam[‡], Yalin Wang[‡], Paul M. Thompson[§], and Tony F. Chan[‡]

Abstract. Surface registration, which transforms different sets of surface data into one common reference space, is an important process which allows us to compare or integrate the surface data effectively. If a nonrigid transformation is required, surface registration is commonly done by parameterizing the surfaces onto a simple parameter domain, such as the unit square or sphere. In this work, we are interested in looking for *meaningful* registrations between surfaces through parameterizations, using prior features in the form of landmark curves on the surfaces. In particular, we generate optimized conformal parameterizations which match landmark curves exactly with *shape-based* correspondences between them. We propose a variational method to minimize a compound energy functional that measures the harmonic energy of the parameterization *maps* and the shape dissimilarity between mapped points on the landmark curves. The novelty is that the computed maps are guaranteed to align the landmark features consistently and give a *shape-based* diffeomorphism between the landmark curves. We achieve this by intrinsically modeling our search space of maps as flows of smooth vector fields that do not flow across the landmark curves. By using the local surface geometry on the curves to define a shape measure, we compute registrations that ensure consistent correspondences between anatomical features. We test our algorithm on synthetic surface data. An application of our model to medical imaging research is shown, using experiments on brain cortical surfaces, with anatomical (sulcal) landmarks delineated, which show that our computed maps give a shape-based alignment of the sulcal curves without significantly impairing conformality. This ensures correct averaging and comparison of data across subjects.

Key words. surface registration, shape-based diffeomorphism, parameterization, conformal, landmark features

AMS subject classifications. 49M99, 92B05, 53B20, 92-08, 30C30

DOI. 10.1137/080738386

1. Introduction. Surface registration is a process of transforming different sets of surface data into one common reference space. It is an important process that allows us to

[†]Department of Mathematics, University of California, Los Angeles, Los Angeles, CA 90095. Current address: Department of Mathematics, Harvard University, 1 Oxford St., Cambridge, MA 02138 (malmlui@math.harvard.edu).

[‡]Department of Mathematics, University of California, Los Angeles, Los Angeles, CA 90095 (sheshadri. thiruvenkadam@ge.com, ylwang@math.ucla.edu, tonyfchan@ust.hk). This work was performed while the last author was on leave at the National Science Foundation as assistant director of the Directorate for Mathematics and Physical Sciences.

[§]Laboratory of Neuro Imaging and Brain Research Institute, UCLA School of Medicine, Los Angeles, CA 90095 (thompson@loni.ucla.edu). This author's research was also supported by grants EB007813, EB008281, AG016570, HD050735, and AG020098.

compare or integrate the surface data obtained from different measurements. It has been studied extensively in different areas of research such as computer vision and medical imaging [1, 2, 6, 19, 20, 23, 33, 49, 53]. For example, surface registration is used to spatially reconcile surface data obtained from different viewpoints, and in this case a rigid transform is sufficient. In medical imaging, surface registration is needed for statistical shape analysis, morphometry, comparing brain surface data, and processing of signals on brain surfaces (e.g., denoising or filtering). In many such applications, a surface must be nonrigidly aligned with another surface, while enforcing higher-order correspondences of features that lie within the two surfaces. Applications include tracking changes over time in geometrical models of anatomy in medical imaging, morphing between shapes while preserving the trajectory of internal features, and reinforcing surface-based signals by combining data from multiple experiments (as in functional imaging of the brain with functional MRI or positron emission tomography, for example).

Usually, surface registration is done by mapping the surfaces into one common simple parameter domain, such as the sphere [8, 11, 12, 39] or a set of two-dimensional (2D) rectangles [42, 45, 46, 48].

Such a process is called parameterization. Parameterization allows us to compare and analyze surface data effectively on the simple parameter domain, instead of considering the complicated surfaces, and this feature is used extensively for numerical grid generation in engineering [28] and to simplify the solutions of PDEs defined on surfaces [29].

In order to compare surface data, surface *diffeomorphisms* that result from parameterizations are often used. For example, if two surfaces are parameterized using the same parameter domain, and the parameterizations are smooth bijective mappings, then a diffeomorphism can be constructed that associates pairs of corresponding points on the two surfaces. For the above diffeomorphisms to map data consistently across surfaces, parameterizations are required that preserve the original surface geometry as much as possible. Parameterizations should also be chosen so that the resulting diffeomorphisms between surfaces align important landmark features consistently. This kind of parameterization, with good feature alignment, is particularly important for medical imaging research examining brain disorders such as Alzheimer's disease and schizophrenia, where systematic features of anatomy and function are identified by building an average brain shape from large numbers of subjects. This is advantageous as the surface average of many subjects would retain, and reinforce, features that consistently occur on sulci (the fissures in the brain surface), while spatially uniform parameterizations of the entire surface, which do not consider these embedded landmarks, may cause these features to cancel out. For an illustration, please see Figure 1.

In this paper, we are interested in looking for parameterizations of surfaces that preserve the local geometry of the surface structure as much as possible while matching the important landmark features exactly based on shape information. These parameterizations let us compute diffeomorphisms to register different surfaces. Many authors have emphasized the value of matching surfaces using diffeomorphisms, as it allows statistics of surface shapes and surface-based signals to be developed by combining information across locations that share the same surface coordinate.

1.1. Previous works. Curve matching and surface registration have been studied extensively by different research groups. We will briefly describe some related methods that are commonly used.

Curve matching has been studied extensively. Younes [51] proposed an elastic matching procedure between plane curves based on computing a minimal deformation cost between the curves. It is done by a variational approach that minimizes a deformation cost which is based on the geodesic distance defined on an infinite-dimensional group acting on the curves. Tagare, O'Shea, and Groisser [37] developed a mathematical theory for establishing correspondences between curves and for nonrigid shape comparison. The proposed correspondences, called bi-morphisms, are more general than those obtained from one-to-one functions. Thiruvenkadam, Groisser, and Chen [38] proposed a variational model to find shape-based correspondences between two sets of level curves. The variational scheme aims at finding a diffeomorphism that minimizes the rate of change of the difference in tangential orientation. While the usual correspondence techniques work with parameterized curves, the authors used a level set formulation that enables the algorithm to handle curves with arbitrary topology. These works focus mainly on finding good diffeomorphisms between one-dimensional (1D) curves in the plane. In our work, we combine surface registration and landmark curve matching on the surface in one model. In other words, we are interested in simultaneously finding a one-to-one correspondence between surfaces while matching landmarks based on the shape information.

Conformal surface registration has been studied widely [3, 4, 21, 22, 24, 25, 35, 41]. In this method, surfaces are parameterized conformally onto simple parameter domains. A diffeomorphism between surfaces can then be easily obtained from the composition of the parameterizations. Conformal parameterization is commonly used for surface registration since it gives a parameterization with minimal angular distortions and provides computational advantages when solving PDEs on surfaces using grid-based and metric-based computations [29]. It is particularly convenient in human brain mapping research to register genus-zero cortical surface models [17, 19]. However, the above parameterization is not guaranteed to map anatomical features, such as sulcal landmarks, consistently from subject to subject [17, 47].

In order to compute a registration between different surfaces that matches important landmark features, landmark-based *diffeomorphisms* [14, 15, 18, 27, 39, 40, 47] are often used to compute, or adjust, surface parameterizations. Optimization of surface diffeomorphisms by landmark matching has been studied by different research groups. Gu et al. [17] optimized the conformal parameterization by composing an optimal Möbius transformation so that it minimizes a landmark mismatch energy. The resulting parameterization remains conformal. Glaunès, Vaillant, and Miller [15] proposed generating large deformation diffeomorphisms of the sphere onto itself, given the displacements of a finite set of template landmarks. The diffeomorphism obtained can match landmark features well, but it is, in general, not a conformal mapping, which can be advantageous for solving PDEs on the resulting grids. Leow et al. [27] proposed a level set–based approach for matching different types of features, including points and 2D or three-dimensional (3D) curves represented as implicit functions, and then these matching fields in the parameter domain were then pulled back onto the surfaces to compute a correspondence field. In related work, Shi et al. [36] computed a direct harmonic mapping between two surfaces by embedding both surfaces as the level set of an implicit function, and representing the mapping energy as a Dirichlet functional in the 3D volume domains. Although such an approach can incorporate landmark constraints, it is not proven to yield diffeomorphic mappings.

Durrleman et al. [9, 10] developed a framework using currents, a concept from differential

geometry, to match landmarks within surfaces across subjects, for the purpose of inferring the variability of brain structure in an image database. Landmark curves are not perfectly matched. This method is good because it allows inexact landmark matching up to a soft constraint. In the case when landmark curves are not entirely accurate, this method is more tolerant of errors in labeling landmarks and gives better parameterization.

Tosun, Rettmann, and Prince [40] proposed a more automated mapping technique that attempts to align cortical sulci across subjects by combining parametric relaxation, iterative closest point registration, and inverse stereographic projection. Wang et al. [47] proposed an energy that computes maps that are close to conformal and are also driven by a landmark matching term that measures the Euclidean distance between the specified landmarks. The resulting map is an optimized conformal map that matches landmarks as much as possible, although not perfectly.

Some authors have proposed driving features into correspondence based on the shape information across surfaces by driving a flow in surface coordinates that minimizes a measure of discrepancy between the signals on the surfaces. For example, Wang, Chiang, and Thompson [42] proposed computing surface registrations which match the mutual information. Pienaar et al. [34] and Lyttelton et al. [32] proposed computing surface parameterizations that match surface curvature. Fischl et al. [12] proposed improving the alignment of the folding patterns of the cortical surface by minimizing the mean squared difference between the average convexity across a set of subjects and that of the individual. These approaches are more automated but do not allow the exact matching of landmarks lying within the surfaces, which often take the form of sets of 3D points or 3D spatial curves that need to be precisely matched. Most of the prior approaches have not dealt with the exact matching of landmarks, which also preserves shape information on the landmark curves. Usually when data are averaged, shape information along the landmarks is canceled out rather than preserved.

1.2. Motivation of our work. As we can see, some of the above earlier methods require pointwise correspondence between feature curves on the surfaces to be labeled in advance [15, 47]. The correspondences obtained may not be sufficiently accurate or reproducible. In addition, some of the other methods often use landmark matching measures based on the Euclidean distance, or the overlap of level set functions representing the landmarks. The correspondences of features within curves are usually not guided by any shape information. Thus, the resulting correspondences would be unreliable in the case of landmark curves that differ by nonrigid deformations (i.e., that cannot be matched using uniform speed parameterizations). Thus, the registration or diffeomorphism between surfaces obtained does not invoke any geometric information. This is especially disadvantageous in human brain mapping when we need to build average brain surface models, with well-defined features, by using the registration. This process is illustrated in Figure 1. Figure 1(A) shows two different surfaces, namely, Surface 1 and Surface 2. Figure 1(B) shows the result of averaging the two surfaces, but using a surface registration that does not take into account the shape information when matching. Note that the shape of the landmarks is averaged out and cannot be preserved. Figure 1(C) shows the averaging result based on surface registrations that contain information on shape correspondence between landmark curves. The shape of the landmark curve is well preserved. Finally, some of the above methods use shape data terms to improve the overall
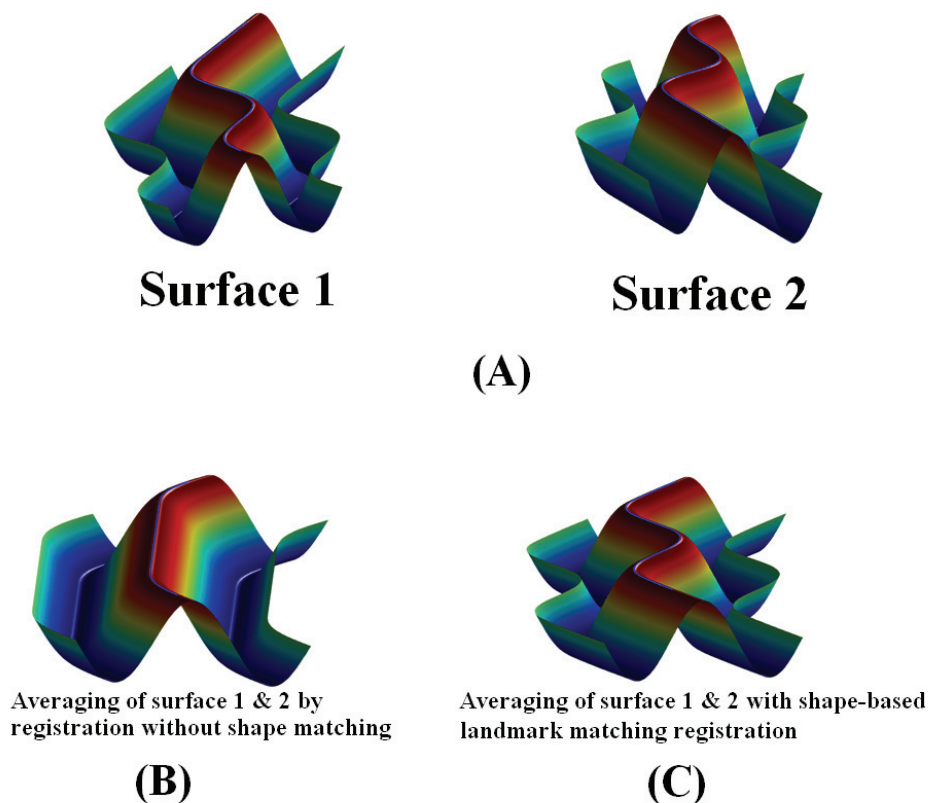
Surface 1   **Surface 2**

(A)

Averaging of surface 1 & 2 by
registration without shape matching

Averaging of surface 1 & 2 with shape-based
landmark matching registration

(B)   **(C)**

Figure 1. (A) *shows two different surfaces, namely, Surface* 1 *and Surface* 2. (B) *shows the result of averaging the two surfaces with a surface registration that does not match shape information. Note that the shape of the landmarks is averaged out and cannot be preserved.* (C) *shows the result of averaging the shapes with a surface registration that incorporates shape correspondences between landmark curves. Note that the shape of the landmark curve is well preserved.*

alignment of patterns based on the shape information. Exact matching of landmark curves based on the shape information cannot be guaranteed. In the situation when landmark curves are not very accurate, it is good to allow inexact landmark matching up to a soft constraint, so as to tolerate landmark error [9, 10]. However, in the case that landmark curves can be consistently and accurately approximated, it might be beneficial to have exact landmark matching so that the resulting average surfaces look "sharp" and have features. For example, in this project, landmark curves are chosen as major sulci on brains. These major sulci, such as the central sulcus, are defined as the deepest curves on the convoluted brain surface, which can be consistently and accurately approximated using a variational approach [30]. Constraining the surface diffeomorphism to exactly align the landmark curves during minimization is difficult; see, e.g., [40, 47].

To resolve the above issues, we propose a method for optimizing the conformal parameterization of the surfaces while nonrigidly registering the landmark curves. As in the above

works, given two surfaces with landmark curves labeled, we want to find close to conformal (i.e., angle-preserving) parameterizations for the surfaces driven by shape-based correspondences (*registration*) between the landmark curves. Specifically, we formulate our problem as a variational energy defined on a search space of diffeomorphisms generated as flows of smooth vector fields. The vector fields are restricted to only those that *do not flow* across the landmark curves (to enforce exact landmark correspondence). Our energy has two terms: (1) a shape term to map similarly shaped segments of the landmark curves to each other and (2) a harmonic energy term to optimize the conformality of the parameterization maps.

Our work has three main contributions: First, the surface diffeomorphism resulting from our parameterization maps the sulcal curves *exactly*. Exact landmark matching registration is helpful in getting sharp average surfaces with features, in the case when landmark curves can be accurately approximated. Of course, when landmark curves are not accurate enough, it might be preferable to allow some degree of inexact landmark matching. Our method can also be easily extended to allow inexact landmark matching up to a soft constraint, by adding a penalty term [10]. Second, the correspondence is shape-based; i.e., it maps similarly shaped segments of sulcal curves to each other. Finally, the conformality of the surface parameterizations is preserved to the greatest possible extent. It is desirable when conformal structure is used for shape analysis. For example, conformal modules can be used to give signatures for different biological shapes [43, 44, 52]. Conformality distortion can be used to detect deformities [31]. Optimized conformal parameterization will be helpful for these purposes. Also, by preserving conformality as much as possible, the local geometry distortion under the map will be minimized.

2. Mathematical background.

2.1. Basic Riemann surface theory.
A Riemann surface means a 1D complex manifold. Mathematically, a Riemann surface (S, g) (with Riemannian metric g) is a real differentiable 2D manifold S in which each tangent space is equipped with an inner product g that varies smoothly from point to point. This allows one to define various notions such as angles, lengths of curves, areas (or volumes), and curvature [5, 6, 26]. Specifically, a vector field $\vec{V} : S \to TS$ on a Riemann surface is a map that assigns a tangent vector for each point on a surface. A Riemannian metric $g = \{g_p\}_{p \in S}$ on S is a family of inner products

$$(2.1) \qquad g_p : T_pS \times T_pS \to \mathbb{R}, \quad p \in S,$$

such that, for all differentiable vector fields X, Y, the application $p \mapsto g_p(X(p), Y(p))$ is differentiable.

Given two Riemann surfaces M and N, a map $f : M \to N$ is *conformal* if it preserves the first fundamental form up to a scaling factor. Mathematically, this means that

$$(2.2) \qquad f^*(ds_N^2) = \lambda(x_1, x_2)ds_M^2.$$

The scaling factor λ is called the *conformal factor*. An immediate consequence is that every conformal map preserves angles. With the angle-preserving property, a conformal map can effectively preserve the local geometry of the surface structure. This is the reason why conformal maps are commonly used for surface registration.

2.2. Integral flow of a smooth vector field. Next, we introduce briefly the concept of the integral flow of a vector field on a Riemann surface.

Let $\vec{V}$ be a smooth vector field on a Riemann surface M which associates a tangent vector to every point on S. Given the vector field $\vec{V}$, we can try to define curves γ on S such that, for each t in an interval I,

$$(2.3) \qquad \gamma'(t) = V(\gamma(t)), \quad \gamma(0) = p.$$

If V is Lipschitz continuous, we can find a unique C^1-curve γ^x for each point x in S so that

$$(2.4) \qquad \gamma'_x(t) = V(\gamma_x(t)) \quad (t \in (-\epsilon, +\epsilon) \subset R), \qquad \gamma^x(0) = x.$$

On a compact Riemann surface S, any smooth vector field $\vec{V}$ is *complete*, meaning that every integral curve is defined for all $t \in R$. We can define a map, called the *integral flow* of $\vec{V}$, $\phi(t, x) : R \times S \to S$, as follows:

$$(2.5) \qquad \phi(t, x) = \gamma_x(t).$$

Fixing t, $\phi^t(x) = \phi(t, x)$ is a diffeomorphism of the surface S. Therefore, we can regard the integral flow as a collection of diffeomorphisms of S. Interestingly, the integral flow follows the group law, meaning that $\phi^t \circ \phi^s(x) = \phi^{s+t}(x)$.

In this work, we consider the search space of diffeomorphisms as the integral of smooth vector fields. By looking for a smooth vector field that satisfies a certain energy functional, we can ensure that the map obtained is a diffeomorphism that matches landmarks based on the shape information.

3. Detection of landmark features. In this work, we are interested in looking for meaningful diffeomorphisms which match geometric features. Geometric features are represented by landmark curves. Usually, the landmark curves can be manually labeled. For example, sulcal landmark curves are labeled manually by neuroscientists in human brain mapping research. Alternatively, automatic detection of landmark curves has been introduced by different research groups. For example, Yoshizawa et al. [50] proposed a method for detecting crest lines on a surface mesh, which are defined by the derivatives of the first and second curvatures. Lui et al. [30] proposed a method for detecting landmark curves based on the principal curvatures. In this paper, we detect the landmark curves on the surface based on Lui's algorithm.

4. Computation of curvatures on the surface. Curvature is an important geometric quantity defined on the surface. In this paper, curvature is used to define the shape measure on landmark curves. Matching curves based on curvatures allows us to match similarly shaped segments of landmark curves to each other. In a neuroscientific point of view, there are brain regions, e.g., the genu of the central sulcus, where a curvature maximum is a guide to a cellular region that is truly homologous in function [7, 16]. It motivates us to define shape measure with curvature to match primary sulci. However, for minor sulci, there is no strong neuroanatomical justification for the curvature matching corresponding anatomy across subjects. In the case when minor sulci are used as landmarks, the shape measure can be suitably modified to better match corresponding anatomy across subjects.

Intuitively, curvature of a space curve measures the amount by which the curve deviates from being a straight line. The curvature κ_n of a space curve is the reciprocal of the radius of the circle lying on the osculating plane that best approximates the curve. It is invariant with respect to reparameterization and is therefore a measure of an intrinsic property of the curve. Mathematically,

$$\kappa_n(\gamma(t)) = \frac{||\gamma'(t) \times \gamma''(t)||}{||\gamma'(t)||^3}.$$

Given a discrete representation $\{\gamma(t_1), \gamma(t_2), \ldots, \gamma(t_n)\}$ of γ, the curvature can be computed as

$$\kappa_n(\gamma(t_i)) = \frac{2||[\gamma(t_{i+1}) - \gamma(t_i)] \times [\gamma(t_{i+1}) - 2\gamma(t_i) + \gamma(t_{i-1})]||}{||\gamma(t_{i+1}) - \gamma(t_i)||||\gamma(t_i) - \gamma(t_{i-1})||||\gamma(t_{i+1}) - \gamma(t_{i-1})||}.$$

5. Model. We are going to describe in detail our proposed model. Given two surfaces M_1 and M_2, we label them with landmark curves $\hat{C}_1$ and $\hat{C}_2$, which provide matching criteria for the models. The curves $\hat{C}_i$ on M_i have the same topology. These landmarks curves are inputs of Algorithm 1 and can be detected automatically or semiautomatically in advance as we describe in section 3. Here, we want to find parameterizations $\hat{f}_1 : \Omega \subset \Re^2 \to M_1$, $\hat{f}_2 : \Omega \to M_2$ of M_1 and M_2, respectively, such that $\hat{f}_2 \circ \hat{f}_1^{-1}|_{\hat{C}_1}$ is a shape-based diffeomorphism onto $\hat{C}_2$. In other words, $\hat{f}_2 \circ \hat{f}_1^{-1}$ maps *similarly shaped* segments of $\hat{C}_1$ and $\hat{C}_2$ to each other. On the other hand, we want $\hat{f}_i$ to be as close to conformal as possible. As a result, the map $\hat{f}_2 \circ \hat{f}_1^{-1}|_{\hat{C}_1}$ obtained is an optimized conformal diffeomorphism before the surfaces are matched with shape-based landmark matching.

In real-world applications, the surfaces we are dealing with are usually complicated, e.g., the cortical surface of the brain. So, it is difficult for us to solve the matching problem directly on these complicated surfaces. To simplify our computations, we propose reducing the problem to a 2D problem formulated on the 2D plane, by parameterizing the surfaces. Specifically, we first parameterize M_i conformally onto the conformal parameter domain D_i. The conformal parameterization can be obtained effectively as described in [48]. Assume that $\hat{C}_i$ are mapped to C_i on the parameter domain D_i. Thus, our problem is reduced to the 2D problem of finding a diffeomorphism $\tilde{f}_i : \Omega \to D_i$ such that $\tilde{f}_2 \circ \tilde{f}_1^{-1}|_{C_1} = C_2$ is a shape-based diffeomorphism onto C_2. We formulate our problem as a variational problem that minimizes an energy functional with respect to diffeomorphisms $\tilde{f}_i : \Omega \to D_i$, subject to the correspondence constraint $\tilde{f}_2 \circ \tilde{f}_1^{-1}(C_1) = C_2$. The energy consists of two terms. The first term measures the harmonic energy of the maps $\tilde{f}_i$, which serves to preserve the conformality of the parameterization as far as possible, and the second term measures the shape dissimilarity between points on C_1 and C_2 that correspond via the maps, which serves to match landmark curves based on the shape information.

In most situations, the geometry of the landmark curves is not simple. Thus, handling the above correspondence constraint may not be easy. In order to simplify the problem, we move all our computations to the parameter domain Ω using initial diffeomorphisms $f_{0,i} : \Omega \to D_i$, which matches the landmark curves C_i to a common simple curve C such as a straight line. This initial diffeomorphism serves as an initial condition, and it does not need to be conformal; nor does it need to have any shape-matching properties. Let $C \subset \Omega$ be a topological representative of C_i. We have $f_{0,i}(C) = C_i$. With the above framework, the energy is formulated over
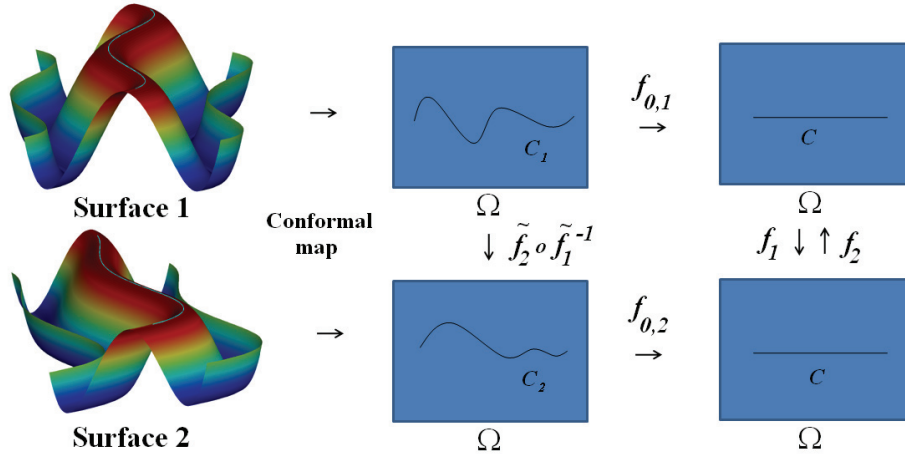
Figure 2. *This figure shows the framework of Algorithm* 1.

Ω, and the search space of diffeomorphisms $\tilde{f}_i : \Omega \to D_i$, subject to $\tilde{f}_2 \circ \tilde{f}_1^{-1}(C_1) = C_2$, can be constructed as time-1 flows of smooth vector fields on Ω that do not flow across C. For the shape term, we measure the shape dissimilarity between the corresponding landmarks, which minimizes the difference in *normal curvatures* on the corresponding pairs of points on C_1 and C_2. The framework of Algorithm 1 is described geometrically in Figure 2.

To summarize, our problem of finding a shape-based landmark diffeomorphism may be described as follows.

Problem 1. *Given the framework described in Figure 2, we are interested in looking for diffeomorphisms $f_i : \Omega \to \Omega$ that satisfy the following properties:*

(i) *Let $\tilde{f}_i = f_{0,i} \circ f_i : \Omega \to D_i$. Then $\tilde{f}_2 \circ \tilde{f}_1^{-1}$ preserves conformality as much as possible.*

(ii) *$f_i(C) = C$, and $\tilde{f}_2 \circ \tilde{f}_1^{-1}$ maps C_1 to C_2 based on the shape information.*

5.1. Formulation. In this subsection, we formulate the energy functional whose minimization leads to the surface diffeomorphism we desire.

Recall that we are interested in looking for a diffeomorphism $\tilde{f}_i : \Omega \to D_i$ such that $\tilde{f}_2 \circ \tilde{f}_1^{-1}$ matches landmarks exactly based on the shape information while preserving the conformality as far as possible. The initial diffeomorphisms $f_{0,i}$ give us a convenient way to perform our computations on the domain Ω. In order to compute diffeomorphisms $\tilde{f}_i : \Omega \to D_i$ with $\tilde{f}_2 \circ \tilde{f}_1^{-1}(C_1) = C_2$, we compute through the unique diffeomorphisms $f_i : \Omega \to \Omega$ with $f_i(C) = C$, satisfying $\tilde{f}_i = f_{0,i} \circ f_i$ (Figure 2). As a result, we can reduce our problem of finding a parameterization from Ω to D_i to the problem of finding suitable diffeomorphisms from Ω to itself. We are going to formulate our problem as a variational problem that minimizes a combined energy functional defined over diffeomorphisms $f_i : \Omega \to \Omega$ with $f_i(C) = C$. The common curve C is chosen to be the straight line joining the two end points of C_i' in the parameter domain. The combined energy functional consists of two important energies:

1. harmonic energy that optimizes the conformality of the diffeomorphism;

2. shape energy that helps to guide the shape-based correspondence between landmark curves.

Denote $\tilde{f}_i = f_{0,i} \text{ o } f_i$, $F = [\tilde{f}_1, \tilde{f}_2]$. The combined energy functional may be defined as follows:

$$(5.1) \qquad E[f_1, f_2] = \int_\Omega |\nabla \tilde{f}_1|^2 \ + |\nabla \tilde{f}_2|^2 \ dx + \lambda \int_C \left(\kappa_1(\tilde{f}_1) - \kappa_2(\tilde{f}_2)\right)^2 |F_x \wedge F_y| \ ds.$$

The first integral is the harmonic energy of $\tilde{f}_i$, which measures the L^2-norm of its gradient. The second term is a *symmetric* shape term defined as an arc length integral over $F(C)$. Algorithm 1 is based on the work of Thiruvenkadam, Groisser, and Chen [38], but is a major extension of that work. In [38], the nonrigid correspondence problem between implicitly defined curves was considered. Our work significantly extends the notion of matching implicit curves to apply it to general 3D surfaces such as models of the cerebral cortex, with the added complication of the nonflat surface metrics. Here, the shape measure $\kappa_i(p_i)$ is determined by the normal curvature of M_i corresponding to the point p_i. By minimizing this energy, we can obtain diffeomorphisms that map similarly shaped segments of the landmark curves to each other. Defining the symmetric shape measure over $F(C)$ makes the term independent of the choice of the initial maps $f_{0,i}$, and also avoids local minima problems that can occur while matching flat curve segments.

In the above energy, using a search space of diffeomorphisms $f_i : \Omega \to \Omega$ and then imposing $f_i(C) = C$ as a constraint during minimization is difficult. Hence we propose a method for directly considering a *reduced search space* of diffeomorphisms $f_i : \Omega \to \Omega$ that satisfy $f_i(C) = C$. We will explain an effective method for describing this reduced search space of diffeomorphisms later.

5.2. Level set representation for C. Note that in our energy functional, the shape measure integral is defined over the curve C. To implement an algorithm that can minimize the energy effectively, this integral has to be reformulated so that it can be defined over the whole parameter domain Ω. This may be done by representing the curve C implicitly—in level set form—so that we can write the second integral in energy (5.1) with respect to $x \in \Omega$. Since we are dealing with curves as our landmarks, we assume that $C = \cup_{k=1}^N \Gamma_k$, a union of open curves $\Gamma_k \subset \Omega$. As the union of open curves, C can be represented as the intersection of the 0-level set of a signed distance function ϕ and a region A (see Figure 3). In other words, we can represent the set of curves C by looking for any choice of a level set function together with a region, such that the intersection of the 0-level set with the region is equal to C. With this construction, the arc length integral of C becomes

$$\int_C \ ds = \int_\Omega \boldsymbol{\chi}_A \ |\nabla H(\phi)| \ dx,$$

where χ_A is the indicator function. As a result, the shape measure integral in the combined energy can be written as

$$\int_\Omega \boldsymbol{\chi}_A \left(\kappa_1(\tilde{f}_1) - \kappa_2(\tilde{f}_2)\right)^2 |\nabla H(\phi)| \ |F_x \wedge F_y| \ dx.$$

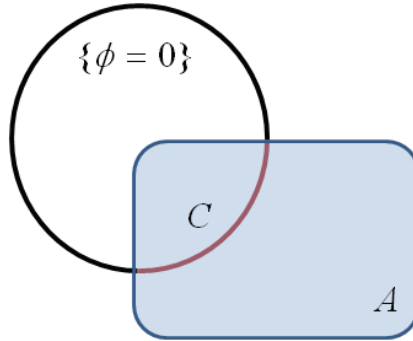# Implicit representation of landmark curves

Figure 3. *This figure shows the level set representation of the landmark curve C (brown open curve), $C = \{\phi = 0\} \cap A$. A is the shaded region; $\{\phi = 0\}$ is the circle. The landmark curve C is represented implicitly to help in formulating the energy functional.*

5.3. Modeling the search space for f_i. Recall that our combined energy functional is defined on a *reduced search space* of diffeomorphisms $f_i : \Omega \to \Omega$ that satisfy $f_i(C) = C$. With our proposed framework, we can describe this reduced search space of diffeomorphisms effectively by using smooth vector fields defined on Ω.

To construct an appropriate search space for f_i, we consider smooth vector fields, $\vec{X}_i = a_i \frac{\partial}{\partial x} + b_i \frac{\partial}{\partial y}$, where $a_i, b_i : \Omega \to \Re$ are C^1 functions with compact support. Then the integral flow of $\vec{X}_i$, $\Phi^{\vec{X}_i}(\mathbf{x}, t)$, is given by the differential equation

$$\frac{\partial \Phi^{\vec{X}_i}}{\partial t}(\mathbf{x}, t) = \vec{X}_i(\Phi^{\vec{X}_i}(\mathbf{x}, t)),$$

$$\Phi^{\vec{X}_i}(\mathbf{x}, 0) = \mathbf{x}.$$

In particular, the time-1 flow $\Phi^{\vec{X}_i}(\mathbf{x}, 1) : \Omega \to \Omega$ is a diffeomorphism from Ω to itself.

To ensure that the time-1 flow of the smooth vector field belongs to the reduced search space of diffeomorphisms, certain constraints must be satisfied by the vector field. Specifically, the vector field on the landmark curve C must be tangent to C to ensure the exact landmark matching. In Algorithm 1, the projection operator is defined as projecting the vector field onto the curve to ensure that the tangential property is satisfied (see Figure 4).

With this setup, the flow of the smooth vector field is a diffeomorphism of Ω which matches C to itself. Figure 5(A) shows the vector field defined on the domain. The vector field on the landmark is tangent to the curve. Figure 5(B) shows the grid lines on the domain. Several points are labeled on the landmark to visualize its displacement under the integral flow. Figure 5(C) shows the result of the integral flow of the vector field. A diffeomorphism with exact landmark matching is obtained. Note that points slide along the landmark curve, instead of flowing across the curve.
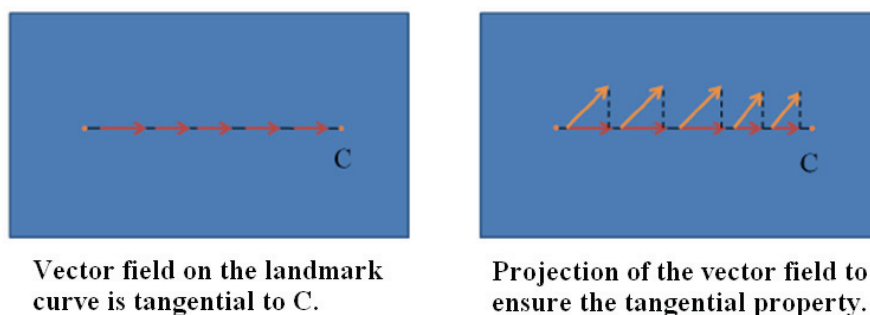
Figure 4. *The vector field on the landmark curve C is tangential to C to ensure exact landmark matching. In Algorithm 1, the projection operator is defined to project the vector field onto the curve to ensure that the tangential property is satisfied.*
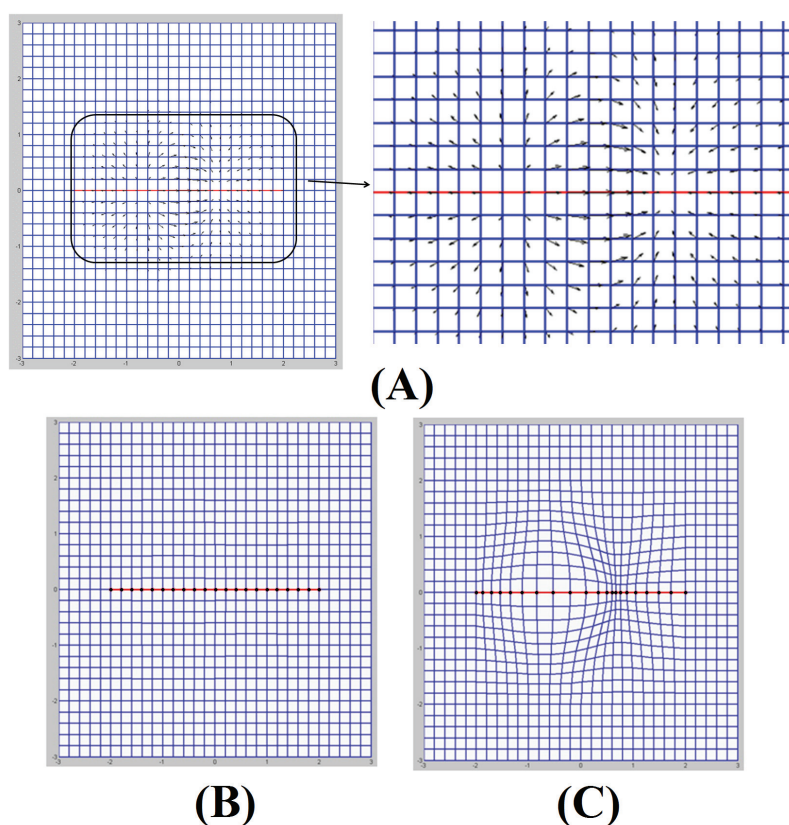

Figure 5. *(A) shows the vector field defined on the domain. The vector field on the landmark is tangential to the curve. (B) shows the grid lines on the domain. Several points are labeled on the landmark to visualize its displacement under the integral flow. (C) shows the result of the integral flow of the vector field. A diffeomorphism with exact landmark matching is obtained. Note that points slide along the landmark curve, instead of flowing across the curve.*

Mathematically, let $\vec{n} := \delta_\epsilon(\phi) \, \chi_A \nabla \phi_\epsilon$. The regularized version of χ_A can be computed as follows: Let B be a subset of $\Omega - A$ such that $\max_{p,q \in \Omega - (A \cup B)} d(p,q) < \alpha$. We set $\chi_A = 1$ in A, $\chi_A = 0$ in B and diffuse it to a smooth function. We see that $\vec{n}$ coincides with the unit-normal vector field on C. Let η_{ep} be a smooth function on Ω such that $\eta_{ep} = 0$ at the end points of the open curves $\Gamma_k \subset C$, $k = 1, 2, \ldots, N$. Consider the vector fields $\vec{Y}_i$ that do not *flow across* C:

$$\vec{Y}_i = P_C X_i := \eta_{ep} \left(\vec{X}_i - (\vec{X}_i \cdot \vec{n}) \vec{n}_i \right).$$

We notice the following properties for the time-1 flow, $\Phi^{\vec{Y}_i}(.,1)$:

- $\Phi^{\vec{Y}_i}(.,1) : \Omega \to \Omega$ is a diffeomorphism since $\vec{Y}_i$ is C^1.
- Also, $\vec{Y}_i|_C$ is a C^1 vector field on C. Thus $\Phi^{\vec{Y}_i}(.,1)|_C$ is a diffeomorphism onto C.

Hence it is natural to set $f_i = \Phi^{\vec{Y}_i}(.,1)$. Note that Algorithm 1 depends on the parameters ϵ, ep, and α. With larger values of these parameters, the conformality distortion near the landmarks will be spread out on a larger region.

5.4. Energy. We formulate the energy (5.1) over the space of C^1 smooth vector fields on Ω, $\vec{X}_i = a_i \frac{\partial}{\partial x} + b_i \frac{\partial}{\partial y}$:

$$J[a_i, b_i] = \int_\Omega |\nabla \tilde{f}_1|^2 \; + |\nabla \tilde{f}_2|^2 \, dx + \lambda \int_\Omega \chi_A \big(\kappa_1(\tilde{f}_1) - \kappa_2(\tilde{f}_2)\big)^2 \, |\nabla H(\phi)| \, |F_x \wedge F_y| \, dx$$

$$(5.2) \qquad\qquad\qquad\qquad\qquad\qquad + \beta \int_\Omega |D\vec{X}_1|^2 + |D\vec{X}_2|^2 \, dx.$$

Here, as before, $\tilde{f}_i = f_{0,i} \circ f_i$, $f_i = \Phi^{\vec{Y}_i}(.,1)$, and the time-1 flow of the vector field $\vec{Y}_i = P_C X_i$. The last integral in the energy is the smoothness term for the vector fields $\vec{X}_i$. The first two integrals are the harmonic terms which aim to preserve the conformality of the parameterization as much as possible. The third integral is the shape term, which ensures that landmarks are matched exactly, based on the shape information. Note that shape measures in the third integral are integrated over Ω. Initially, shape measures are defined on the curves. They are smoothly extended to be defined on Ω by iterative diffusion, while fixing their values on landmark curves. The last integral in the energy is the smoothness term, which ensures that the minimizing vector fields $\vec{X}_i$ are smooth.

6. Derivation of the iterative scheme on vector fields. In this section, we will describe in detail how we can implement Algorithm 1 to minimize the proposed energy functional. This can be done by iteratively modifying the vector fields according to the Euler–Lagrange equation of the energy functional.

Recall that in this work, we formulate the energy functional over the space of C^1 smooth vector fields $\vec{X}_i$ on Ω.

Theorem 1. *Denote $\vec{X}_i = a_i \frac{\partial}{\partial x} + b_i \frac{\partial}{\partial y}$. Our energy functional (5.2) is formulated over the space of C^1 smooth vector fields $\vec{X}_i$ on Ω.*

Equation (5.2) can be minimized iteratively by the following equation:

$$\frac{d}{dt} X^i(t) = \left(\frac{da_i}{dt}, \frac{db_i}{dt} \right),$$

where

$$\frac{da_i}{dt} = \int_0^1 B_i(\phi_s^{\vec{Y}_i}) \; \Psi_i(\phi_s^{\vec{Y}_i}, 1) \; \Psi_i^{-1}(\phi_s^{\vec{Y}_i}, s) \; P_C \vec{e}_1 \; |D\phi_s^{\vec{Y}_i}| \; ds - 2\beta \Delta a_i,$$

$$\frac{db_i}{dt} = \int_0^1 B_i(\phi_s^{\vec{Y}_i}) \; \Psi_i(\phi_s^{\vec{Y}_i}, 1) \; \Psi_i^{-1}(\phi_s^{\vec{Y}_i}, s) \; P_C \vec{e}_2 \; |D\phi_s^{\vec{Y}_i}| \; ds - 2\beta \Delta b_i,$$

where $B_i := -2\Delta \tilde{f}_i \; Df_{0,i} \; + \; \lambda \boldsymbol{\chi}_A \left((-1)^{i-1} 2\big(\kappa_1(\tilde{f}_1) - \kappa_2(\tilde{f}_2)\big) \nabla \kappa_i - \nabla \cdot C_i\right) Df_{0,i} \; |\nabla H(\phi)|$
and Ψ_i *is the orthogonal fundamental matrix for the homogeneous system of*

$$\frac{\partial}{\partial t} P_i(\vec{x}, t) = \eta P_C \vec{e}_1 \; (\Phi^{\vec{Y}_i}(\vec{x}, t)) + D\vec{Y}_i(\Phi^{\vec{Y}_i}(\vec{x}, t)) \; P_i(\vec{x}, t), \quad P_i(\vec{x}, 0) = \mathbf{0}.$$

Proof. Let $D_v^\eta F = \frac{d}{d\epsilon} F(v + \epsilon \eta)$ denote the derivative of a functional F with respect to variable v, and for variation η. Also denote the vector fields $\vec{e}_1 := \frac{\partial}{\partial x}$, $\vec{e}_2 := \frac{\partial}{\partial y}$. It follows that

$$D_{a_i} J(\eta) = -2 \int_\Omega \Delta \tilde{f}_i \; Df_{0,i} \; D_{a_i}^\eta f_i \; dx + 2\lambda \int_\Omega \boldsymbol{\chi}_A (-1)^{i-1} \big(\kappa_1(\tilde{f}_1) - \kappa_2(\tilde{f}_2)\big)$$

$$\cdot \nabla \kappa_i Df_{0,i} \; D_{a_i}^\eta f_i |\nabla H(\phi)| \; |F_x \wedge F_y| \; dx + \lambda \int_\Omega \boldsymbol{\chi}_A \big(\kappa_1(\tilde{f}_1) - \kappa_2(\tilde{f}_2)\big)^2$$

$$\cdot \frac{1}{|F_x \wedge F_y|}(|F_y|^2 F_x \cdot D_{a_i}^\eta F_x + |F_x|^2 F_y \cdot D_{a_i}^\eta F_y - (F_x \cdot F_y)(F_x \cdot D_{a_i}^\eta F_y + F_y \cdot D_{a_i}^\eta F_x))$$

$$(6.1) \hspace{6cm} \cdot |\nabla H(\phi)| dx - 2\beta \int_\Omega \Delta a_i \; \eta \; dx.$$

Integrating the third term by parts gives

$$-\lambda \int_\Omega \boldsymbol{\chi}_A \nabla \cdot \left((\kappa_1(\tilde{f}_1) - \kappa_2(\tilde{f}_2))^2 \frac{1}{|F_x \wedge F_y|} [|F_y|^2 \partial_x f_i - (F_x \cdot F_y)\partial_y f_i; \right.$$

$$(6.2) \hspace{4cm} |F_x|^2 \partial_y f_i - (F_x \cdot F_y)\partial_x f_i] \Bigg) |\nabla H(\phi)| Df_{0,i} \; D_{a_i}^\eta f_i dx.$$

In the first two integrals, the term $D_{a_i}^\eta f_i$ is given by the flow equation of $\vec{Y}_i = P_C X_i$:

$$\frac{\partial \Phi^{\vec{Y}_i}}{\partial t}(\vec{x}, t) = \vec{Y}_i(\Phi^{\vec{Y}_i}(\vec{x}, t)),$$

$$\Phi^{\vec{Y}_i}(\vec{x}, 0) = x.$$

Now, computing the derivative with respect to a_i on both sides, for variation η, gives the differential equation $P_i := D_{a_i}^\eta \Phi^{\vec{Y}_i}$, which satisfies

$$\frac{\partial}{\partial t} P_i(\vec{x}, t) = \eta P_C \vec{e}_1 \; (\Phi^{\vec{Y}_i}(\vec{x}, t)) + D\vec{Y}_i(\Phi^{\vec{Y}_i}(\vec{x}, t)) \; P_i(\vec{x}, t),$$

$$(6.3) \hspace{7cm} P_i(\vec{x}, 0) = \mathbf{0}.$$

Since $D\vec{Y}_i(\Phi^{\vec{Y}_i}(\vec{x},t))$ is continuous with respect to t, we have the existence of an orthogonal fundamental matrix Ψ_i for the homogeneous system of (6.3). Then a solution for the above problem can be easily verified to be

$$P_i(\vec{x},t) = \Psi_i(\vec{x},t) \int_0^t \Psi_i^{-1}(\vec{x},s) P_C\vec{e}_1 \ (\Phi^{\vec{Y}_i}(\vec{x},s))\eta(\Phi^{\vec{Y}_i}(\vec{x},s)) \ ds.$$

We let $B_i := -2\Delta\tilde{f}_i \ Df_{0,i} \ + \ \lambda\chi_A \left((-1)^{i-1}2(\kappa_1(\tilde{f}_1) - \kappa_2(\tilde{f}_2))\nabla\kappa_i - \nabla\cdot C_i\right) \ Df_{0,i} \ |\nabla H(\phi)|$, where $C_i = (\kappa_1(\tilde{f}_1) - \kappa_2(\tilde{f}_2))^2 \ \frac{1}{|F_x \wedge F_y|}[|F_y|^2\partial_x f_i - (F_x \cdot F_y)\partial_y f_i \ ; |F_x|^2\partial_y f_i - (F_x \cdot F_y)\partial_x f_i]$. Substituting $D^\eta_{X_i} f_i = P_i(.,1)$ in (6.1), we have

$$D_{a_i}J(\eta) = \int_\Omega B_i(\vec{x}) \ \Psi_i(\vec{x},1) \int_0^1 \Psi_i^{-1}(\vec{x},s) \ P_C\vec{e}_1 \ (\Phi^{\vec{Y}_i}(\vec{x},s)) \ \eta(\Phi^{\vec{Y}_i}(\vec{x},s)) \ ds \ dx - \int_\Omega \Delta a_i \ \eta \ dx.$$

For a fixed s, $\Phi^{\vec{Y}_i}(y,s) : \Omega \to \Omega$ is a diffeomorphism; denote the inverse map by $\phi_s^{\vec{Y}_i}$ and its Jacobian by $|D\phi_s^{\vec{Y}_i}|$. A change of variables $(\vec{x},s) \to (y = \Phi^{\vec{Y}_i}(\vec{x},s),s)$ in the first term gives

$$\int_\Omega B_i(\phi_s^{\vec{Y}_i}(y)) \int_0^1 \Psi_i(\phi_s^{\vec{Y}_i}(y),1) \ \Psi_i^{-1}(\phi_s^{\vec{Y}_i}(y),s) \ P_C\vec{e}_1 \ (y) \ |D\phi_s^{\vec{Y}_i}(y)| \ \eta(y) \ ds \ dy.$$

Thus the Euler–Lagrange equations are

$$\frac{da_i}{dt} = \int_0^1 B_i(\phi_s^{\vec{Y}_i}) \ \Psi_i(\phi_s^{\vec{Y}_i},1) \ \Psi_i^{-1}(\phi_s^{\vec{Y}_i},s) \ P_C\vec{e}_1 \ |D\phi_s^{\vec{Y}_i}| \ ds - 2\beta\Delta a_i,$$

$$\frac{db_i}{dt} = \int_0^1 B_i(\phi_s^{\vec{Y}_i}) \ \Psi_i(\phi_s^{\vec{Y}_i},1) \ \Psi_i^{-1}(\phi_s^{\vec{Y}_i},s) \ P_C\vec{e}_2 \ |D\phi_s^{\vec{Y}_i}| \ ds - 2\beta\Delta b_i. \quad\blacksquare$$

To summarize, the algorithm for computing the optimized shape-based landmark matching conformal diffeomorphisms between cortical surfaces is the following.

Algorithm 1. **Shape-based landmark matching diffeomorphism.**

Input : Conformal parameterization $\phi_1 : S_1 \to D_1$, $\phi_2 : S_2 \to D_2$ of S_1 and S_2, respectively. Initial maps $f_{0,1} : D_1 \to \Omega$, $f_{0,2} : D_2 \to \Omega$, time step dt, energy threshold ε, β.

Output : Optimized shape-based landmark matching conformal diffeomorphisms $G_{1,2} : S_1 \to S_2$ and $G_{2,1} : S_2 \to S_1$.

1. Set $n = 0$. Set $\vec{X}_i^0 = (a_i^0, b_i^0) = (0,0)$ everywhere on Ω for $i = 1,2$. Compute energy $E_0 = E[f_1, f_2]$.

2. Compute $\vec{Y}_i^n = P_C\vec{X}_i$; $\phi_S^{\vec{Y}_i^n} : \Omega \to \Omega$; orthogonal fundamental matrix Ψ_i^n; $B_i(\phi_S^{\vec{Y}_i^n})$ for $i = 1,2$.

3. Update (a_i^n, b_i^n) by

$$a_i^{n+1} = \left[\int_0^1 B_i(\phi_s^{\vec{Y}_i}) \ \Psi_i(\phi_s^{\vec{Y}_i},1) \ \Psi_i^{-1}(\phi_s^{\vec{Y}_i},s) \ P_C\vec{e}_1 \ |D\phi_s^{\vec{Y}_i}| \ ds - 2\beta\Delta a_i\right]dt + a_i^n,$$

$$b_i^{n+1} = \left[\int_0^1 B_i(\phi_s^{\vec{Y}_i}) \ \Psi_i(\phi_s^{\vec{Y}_i},1) \ \Psi_i^{-1}(\phi_s^{\vec{Y}_i},s) \ P_C\vec{e}_2 \ |D\phi_s^{\vec{Y}_i}| \ ds - 2\beta\Delta b_i\right]dt + b_i^n.$$

4. Compute energy $E_{n+1} = E[f_1, f_2]$.

5. If $E_{n+1} - E_n < \varepsilon$, stop and return $G_{1,2} = \phi_2^{-1} \circ f_{0,2}^{-1} \circ f_2 \circ f_{0,1}^{-1} \circ \phi_1$, $G_{2,1} = \phi_1^{-1} \circ f_{0,1}^{-1} \circ$ $f_1 \circ f_{0,2}^{-1} \circ \phi_2$. Otherwise, repeat steps 2–4.

7. Numerical implementation of Algorithm 1. In this section, we describe how the proposed algorithm can be implemented. In practice, all surfaces are represented by meshes which consist of vertices, edges, and triangular faces. The functions and their partial derivatives in the iterative scheme are defined on each vertex and linearly interpolated to define the value inside each triangular face. They can be computed as follows:

- Laplacian of a function F can be computed as $\Delta F = \sum_{[u,v] \in N_v} k_{uv}(F(v) - F(u))$, where N_v is a set of triangles around v that forms a neighborhood of v; $k_{uv} = (\cot \alpha + \cot \beta)/2$, where α and β are the opposite angles of the edge $[u,v]$. For details, see [35].

- Gradient $\nabla \kappa_i$ can be computed as $\nabla \kappa_i = \sum_{[u,v,w] \in N_v} \frac{\nabla_{[u,v,w]} \kappa_i}{n}$, where $\nabla_{[u,v,w]} \kappa_i$ is the gradient of κ_i on the triangle $[u,v,w]$. The value of κ_i on $[u,v,w]$ is linearly interpolated. n is the number of faces in N_v.

- $Df_{0,i}$ is defined as $Df_{0,i} = (\nabla f_{0,i}^1, \nabla f_{0,i}^2)$, which is a 2×2 matrix, where $f_{0,i} = (f_{0,i}^1, f_{0,i}^2)$. Similarly, $DY_i := (\nabla \vec{Y}_i^1, \nabla \vec{Y}_i^2)$, where $\vec{Y}_i = (Y_i^1, Y_i^2)$.

- The orthogonal fundamental matrix $\Psi_i(\vec{x}, s)$ is defined as

$$\Psi_i(\vec{x}, s) := \exp\left(\int_0^s D\vec{Y}_i(\Phi^{\vec{Y}_i}(\vec{x}, t)) dt\right).$$

Suppose the interval $[0,1]$ is discretized as $s_0 = 0 < s_1 < \cdots < s_n = 1$. $\Psi_i(\vec{x}, s)$ can be computed as

$$\Psi_i(\vec{x}, s_k) := \exp\left(\sum_{j=1}^k D\vec{Y}_i(\Phi^{\vec{Y}_i}(\vec{x}, s_j))(s_j - s_{j-1})\right).$$

- The function δ_ϵ is defined to be a positive function that is compactly supported in $(-\epsilon, \epsilon)$ and can be computed mathematically as $\delta_\epsilon(x) = \frac{1}{a(\epsilon)\sqrt{\pi}} \exp(-\frac{x^2}{a(\epsilon)^2})$.

- η_{ep} is a smooth function on Ω such that $\eta_{ep} = 0$ at the end points of the open curves $\Gamma_k \subset C$, $k = 1, 2, \ldots, N$. It can be computed mathematically as $\eta_{ep} = 1 - \sum_{i=1}^{2N} \delta_\epsilon^i(x)$, where $\delta_\epsilon^i(x) = \exp(-(x - a_i)/\epsilon^2)$ and $a_1, a_2, \ldots, a_{2N}$ are the set of end points of the landmark curves.

- The initial map f_{0i} maps the landmark curves C_i to the common curve $C_{standard,i}$. It can be computed as follows: Given a set of landmark curves $C_i(t)$ on the parameter domain and a set of corresponding common curves $C_{standard,i}(t)$, starting from the initial map $f_0 = \mathbf{Id}$, we can iteratively flow the map to get a diffeomorphism which matches $C_i(t)$ to $C_{standard,i}(t)$. We can define a vector field on $f^n(C_i(t))$ as $\vec{V}^n(t) = C_{standard,i}(t) - f^n(C_i(t))$ and smoothly extend to the parameter domain by iterative diffusion while fixing the values on the landmark curves. The iterative scheme can then be written as $f^{n+1} = f^n + dt\vec{V}_n(f^n)$.

8. Experimental result. We tested Algorithm 1 on synthetic surfaces with boundaries. Here, we set the vector field to be zero on the boundary. Figure 6 shows the result of matching synthetic surfaces with two sharp corners. Figure 6(A) shows a synthetic surface. It is mapped to another synthetic surface through parameterizations without the shape-based correspondence between landmark curves, as shown in Figure 6(B). The correspondence between the landmark curves does not follow the shape information (see the yellow dots). Figure 6(C) shows the result of matching using our proposed algorithm. Note that the correspondence between the landmark curves follows the shape information (corners to corners; see the yellow dots). Figure 7 shows the matching result of the synthetic surfaces with three sharp corners. Figure 7(A) shows one synthetic surface with three sharp corners. Again, it is mapped to another synthetic surface through parameterizations without the shape-based correspondence between landmark curves, as shown in Figure 7(B). The correspondence between the landmark curves does not follow the shape information. Figure 7(C) shows the result of matching using our proposed algorithm. The correspondence between the landmark curves follows the shape information.

Figure 8 examines qualitatively the performance of our proposed algorithm in matching landmark curves based on the shape information. Figures 8(A) and 8(B) show two surfaces labeled with five landmarks which have similar shapes. Figure 8(A) is taken as a control. We apply Algorithm 1 to map a set of ten similar surfaces, such that the landmarks are matched exactly to each other based on the shape information. Corners (black dots) of the landmark curves are labeled. The surface registration computed with Algorithm 1 matches landmarks based on the shape information, and so the distance between the corresponding corners should be small. Figure 8(C) shows the average percentage error of the distance between feature points (black dots). The distance decreases significantly as the iteration increases.

To examine the conformality of the parameterization, we show in Figure 9 the value of the Beltrami coefficient of the surface parameterizations computed with our proposed algorithm. Six different surfaces (each labeled with five different landmark curves) are mapped to a control surface with similar shape. The Beltrami coefficients of the mappings are computed. The Beltrami coefficient is a measure of conformality of a mapping. It has been commonly used in conformal and quasi-conformal geometry to detect conformality distortion [13]. Given a mapping $f : S_1 \to S_2$, let $\tilde{f} = \varphi_1 \circ f \circ \varphi_2^{-1} : \Omega \subset \mathbb{C} \to \mathbb{C}$, where φ_i is the global conformal parameterization of S_i. The Beltrami coefficient μ_f can be computed as $\mu_f = \tilde{f}_{\bar{z}}/\tilde{f}_z = (\frac{\partial f}{\partial x} + i\frac{\partial f}{\partial y})/(\frac{\partial f}{\partial x} - i\frac{\partial f}{\partial y})$. If f is conformal, $\mu_f = 0$ by the Cauchy–Riemann equation. In Figure 9, the colormap is based on the value of $|\mu_f|$. Note that $|\mu_f|$ is close to zero at most parts of the surfaces, except for the regions near the landmark curves. In other words, conformality distortion occurs only near the landmark curves.

The result of the surface parameterization relies on the parameter ϵ of the delta function δ_ϵ. In order to illustrate how the parameter affects the result of Algorithm 1, we plot the value of the Beltrami coefficient on the surface under different values of ϵ. Figure 10 shows the colormap of $|\mu_f|$ of the surface parameterizations under $\epsilon = 0.2$, $\epsilon = 0.1$, and $\epsilon = 0.02$ (from left to right). Note that as ϵ decreases, the region of conformality distortion decreases. However, the value of $|\mu_f|$ near the landmark curves increases, meaning that more conformality distortion occurs. This is reasonable since the conformality distortion cannot be spread throughout a larger region as ϵ decreases.
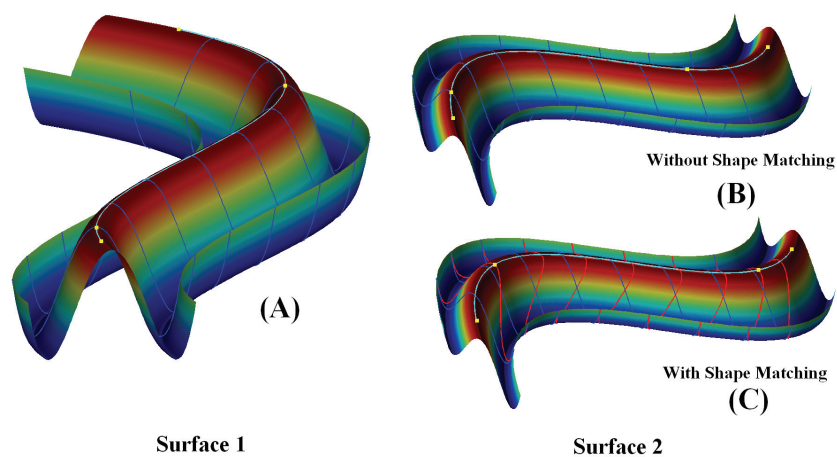
Figure 6. *Testing of Algorithm 1 on synthetic data. The figure shows the result of matching the synthetic data with two sharp corners.*
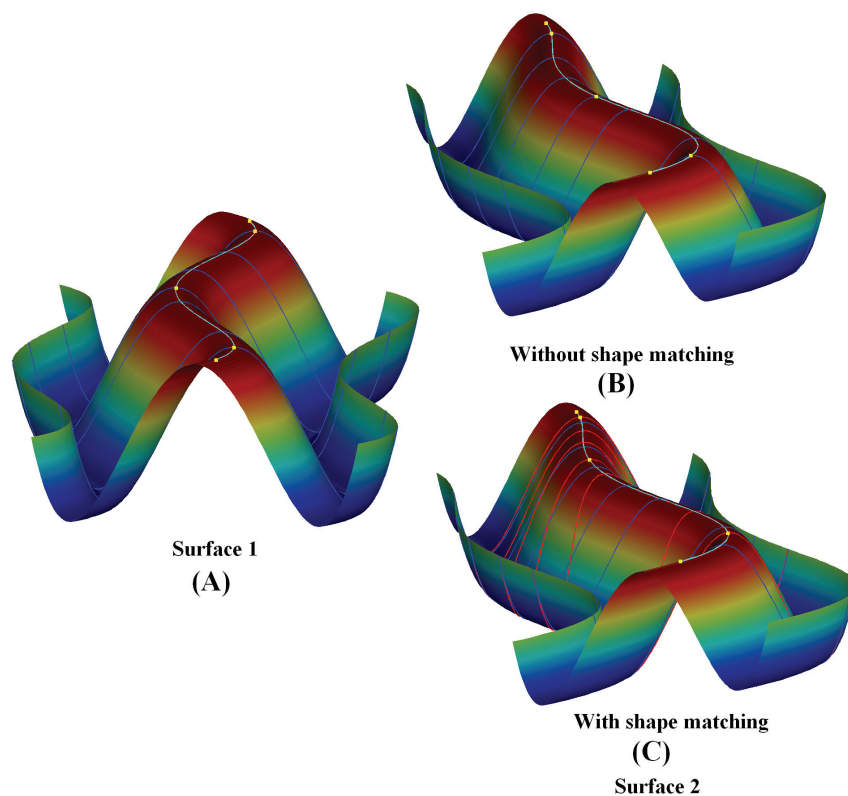
Figure 7. *Another test of Algorithm 1 on additional synthetic data. The figure shows the result of matching synthetic data with three sharp corners.*
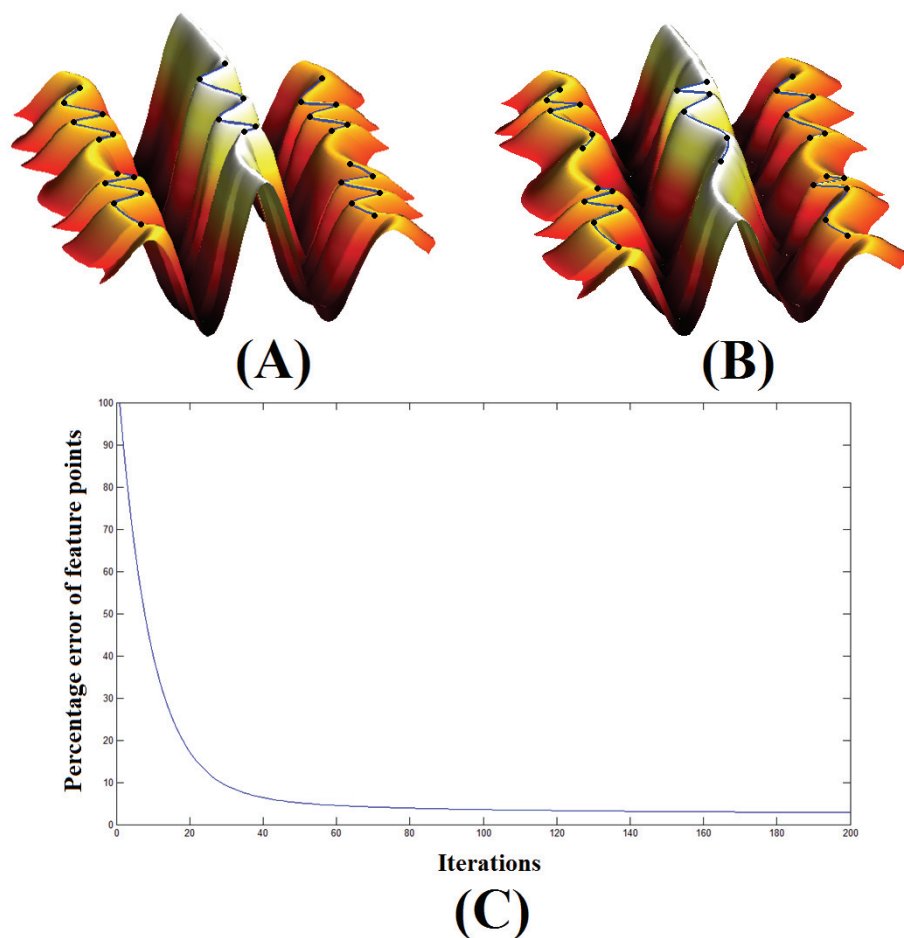
Figure 8. (A) *and* (B) *show two surfaces labeled with five landmarks, which have similar shapes.* (A) *is taken as a control. We apply Algorithm* 1 *to map a set of ten similar surfaces, such that the landmarks are matched exactly to each other based on the shape information.* (C) *shows the average percentage error of the distance between feature points (black dots).*

Table 1 shows the effect of the parameter λ in the energy functional on the surface registration results. It shows the statistics of $Dist$ and $\max|\mu|$ with different λ. Here, $Dist$ is the distance between the corresponding feature points (sharp corners). As λ increases, $Dist$ decreases, meaning that the landmark curves are increasingly matched based on the shape information. However, $\max|\mu|$ increases as λ increases, meaning that more and more conformality is lost near the landmark curves.

We also studied the Jacobian matrix of the deformation under our proposed algorithm. Figure 11 shows the variation of the Jacobian distortion under different lengths and different numbers of landmark curves. Let J be the Jacobian matrix of the surface registration f between the control surface and the other surface with landmarks labeled. The Jacobian distortion is defined as $||J - I||^2$, where I is the identity matrix. The average Jacobian distortion
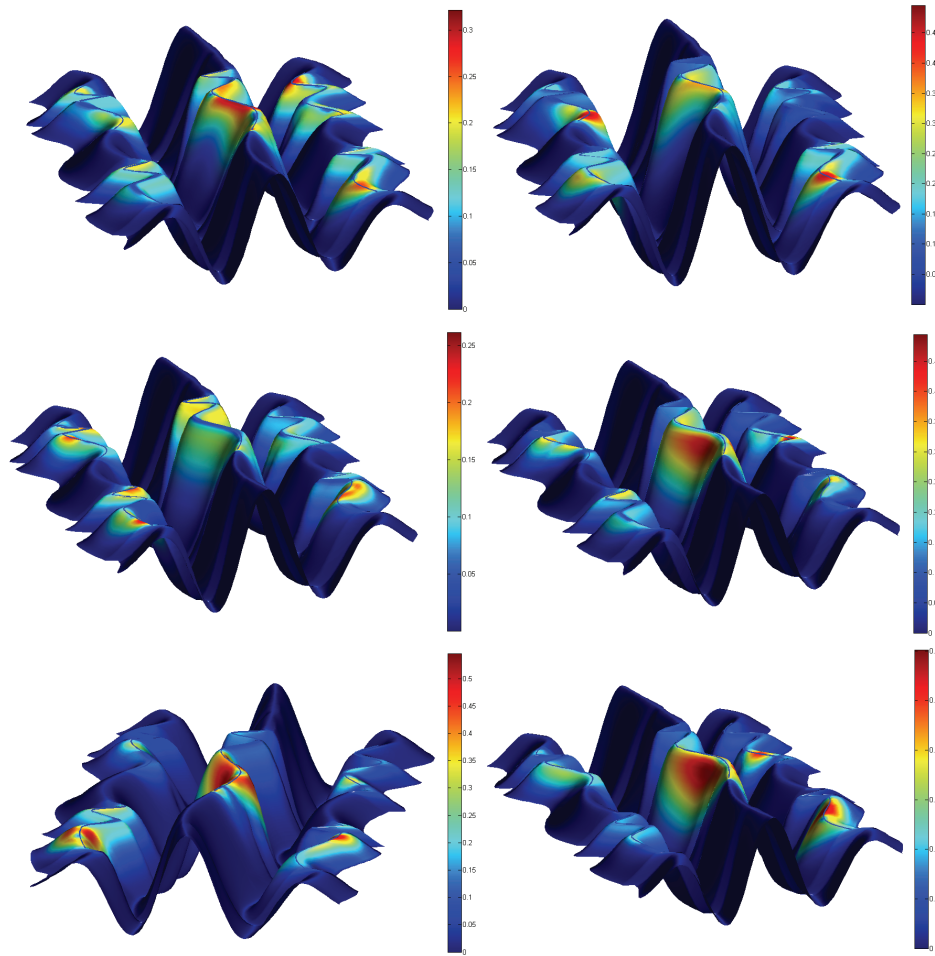
Figure 9. *The figure shows the conformality of the surface parameterizations. Six different surfaces with five landmarks are mapped to a control surface with similar shape. The Beltrami coefficients μ of surface parameterizations are computed. The colormap is based on the value of $|\mu|$. The map is conformal when $|\mu| = 0$. Note that conformality distortion occurs near the landmarks.*
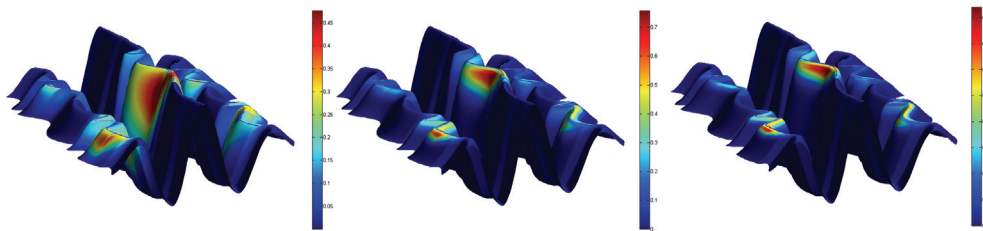

Figure 10. *The figure illustrates how the parameter ϵ of the delta function δ_ϵ affects the result of Algorithm 1: We plot the value of the Beltrami coefficient on the surface under different values of ϵ. The figure shows the colormap of $|\mu_f|$ of the surface parameterizations under $\epsilon = 0.2$, $\epsilon = 0.1$, and $\epsilon = 0.02$ (from left to right). Note that as ϵ decreases, the region of conformality distortion decreases. However, the value of $|\mu_f|$ near the landmark curves increases, meaning that more conformality distortion occurs.*

Table 1

Statistics of Dist and max$|\mu|$ *with different* λ. *Dist is the distance between the corresponding feature points (sharp corners).*

λ	$Dist$	max$|\mu|$	λ	$Dist$	max$|\mu|$
0.1	17.1687	0.4871	2	0.2966	0.5662
0.2	4.5308	0.5458	3	0.1968	0.5685
0.3	2.2354	0.5563	4	0.1470	0.5709
0.4	1.5571	0.5593	5	0.1173	0.5738
0.5	1.2218	0.5607	6	0.0975	0.5771
0.6	1.1016	0.5616	7	0.0834	0.5811
0.7	0.8625	0.5623	8	0.0728	0.5861
0.8	0.7523	0.5628	9	0.0647	0.5926
0.9	0.6671	0.5632	10	0.0582	0.6011
1	0.5992	0.5636	11	0.0530	0.6128

is defined as $\int_S ||J - I||^2 / \int_S dS$. The left-hand plot shows the average Jacobian distortion versus the maximum percentage difference in lengths of landmark curves. As expected, the greater the length difference between corresponding landmarks, the greater the average Jacobian distortion. The right-hand plot shows the average Jacobian distortion versus the number of landmark curves. When the number of landmark curves increases, the average Jacobian distortion increases as well. In addition, we studied the distribution of the Jacobian distortion. Figure 12 shows the Jacobian distortion of the surface parameterizations of different surfaces with five landmarks. The colormap is based on the value of the Jacobian distortion. The result shows that the Jacobian distortion accumulates near landmark curves.

We also illustrate the application of Algorithm 1 by applying it to real brain cortical hemispheric surfaces extracted from brain MRI scans, acquired from normal subjects at 1.5 T (on a GE Signa scanner). Experimental results show that Algorithm 1 can effectively compute cortical surface parameterizations that align the landmark features in a way that also enforces shape correspondence, while preserving the conformality of the surface-to-surface mapping to the greatest extent possible. The computed map is guaranteed to be a diffeomorphism because the map is formulated as the integral flow of a smooth vector field.

Figure 13 shows two different cortical surfaces with sulcal landmarks labeled. We seek parameterizations of these surfaces that align the landmark features consistently while optimally preserving conformality. A diffeomorphism between the two surfaces is then obtained by composing the two parameterizations. Figure 14 shows the result of matching the cortical surfaces with one landmark labeled (for purposes of illustration) on each brain. Figure 14(A) shows the cortical surface of Brain 1. It is mapped to the cortical surface of Brain 2 under the conformal parameterization, as shown in Figure 14(B). Note that the sulcal landmark on Brain 1 is mapped only approximately to the sulcal region on Brain 2. It is not mapped exactly to the corresponding sulcal landmark on Brain 2. Figure 14(C) shows the matching result under the parameterization we propose in this paper. The corresponding landmarks are mapped exactly. Also, the correspondence between the landmark curves follows the shape information. It maps the secondary features of one landmark curve to the secondary features of the other landmark curve (see the black dots). Figures 14(D) and 14(E) show the standard 2D parameter domain of Brain 1 and Brain 2, respectively. The landmark curve is mapped
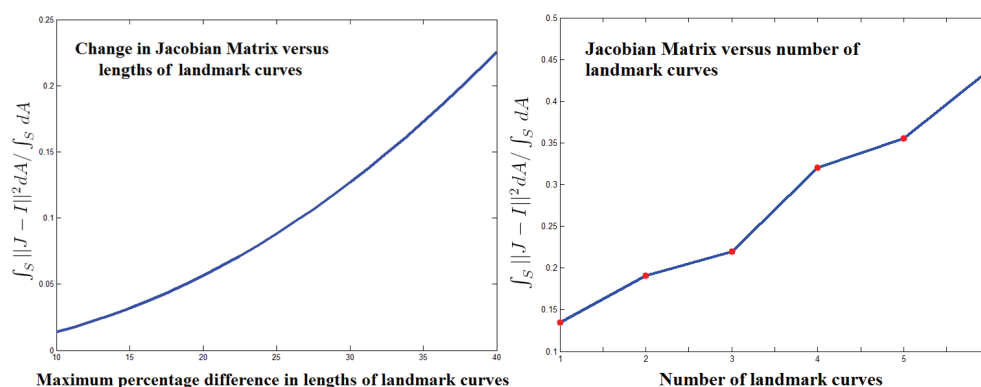
Figure 11. *The variation of Jacobian distortion under different lengths and different numbers of landmark curves. The left-hand plot shows the average Jacobian distortion versus the maximum percentage difference in lengths of landmark curves. The right-hand plot shows the average Jacobian distortion versus the number of landmark curves.*
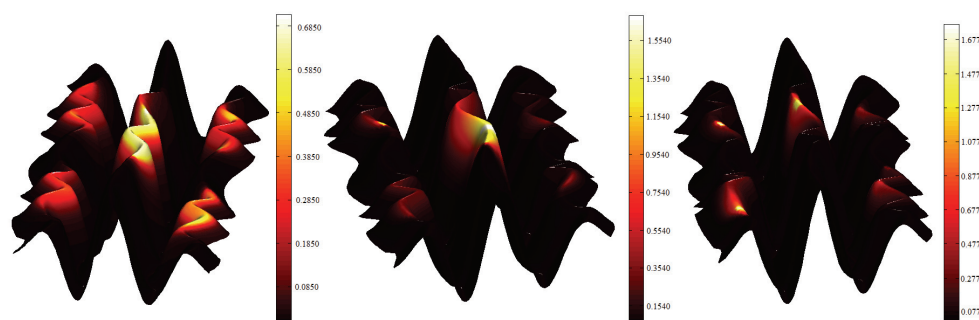

Figure 12. *The figure shows the Jacobian distortion of the surface parameterizations with five landmarks. The colormap is based on the value of the Jacobian distortion. Note that the Jacobian distortion accumulates near the landmarks as expected.*

to the same horizontal line, and the shape features are mapped to the same positions (see the black dots). This is advantageous as the surface average of many subjects would retain features that consistently occur on sulci, while uniform speed parameterizations may cause these features to cancel out (see Figure 1 for an illustration).

Figure 15 illustrates the matching results for cortical surfaces with several sulcal landmarks labeled. Figure 15(A) shows brain surface 1 with several landmarks labeled. It is mapped to brain surface 2 under the conformal parameterization as shown in Figure 15(B). Again, the sulcal landmarks on Brain 1 are mapped only approximately to the sulcal regions on Brain 2. Figure 15(C) shows the matching result under the parameterization we proposed. The corresponding landmarks are mapped exactly. Also, the correspondence between the landmark curves follows the shape information (corners to corners; see the black dots). Figure 16 shows that the shape energy is decreasing with iterations, implying an improving shape-based correspondence between the landmark curves.

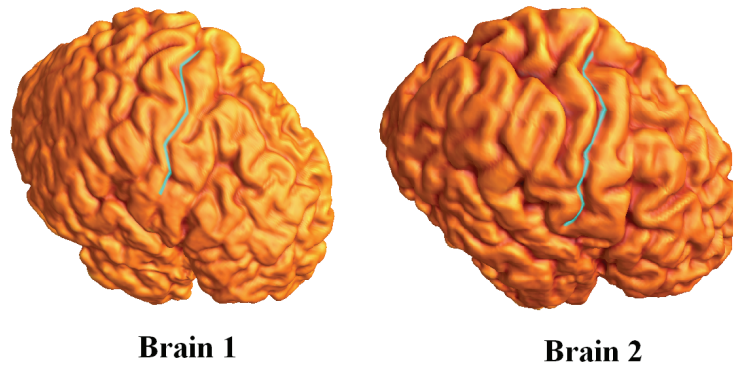Our experiments are carried out on a laptop with 2.4 GHZ DUO CPU and 3G RAM. For

Brain 1   **Brain 2**

Figure 13. *The figure shows two different cortical surfaces. Both brain surfaces are labeled with sulcal landmark curves. We are interested in looking for a diffeomorphism between them which matches landmark curves exactly based on the shape information.*
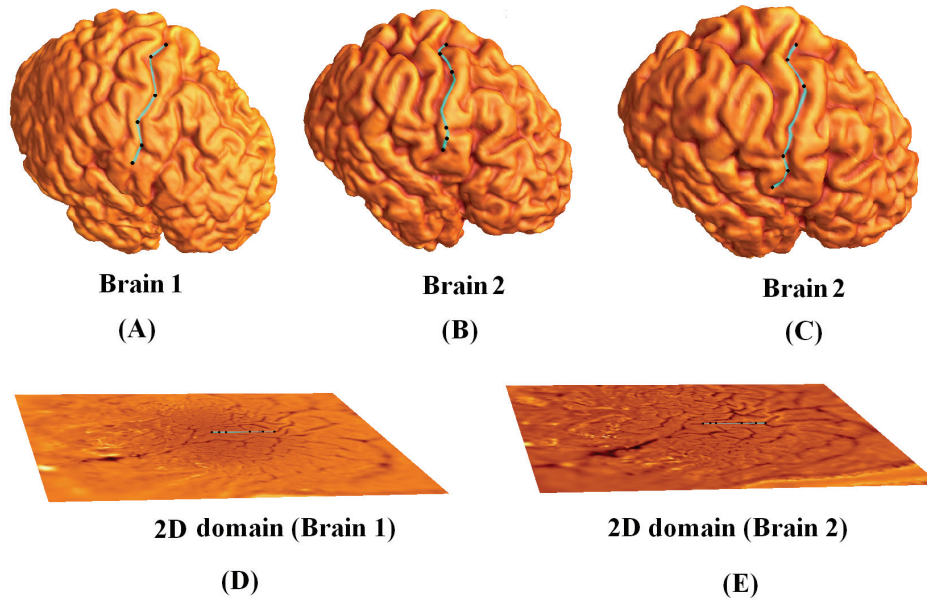

Brain 1   **Brain 2**   **Brain 2**

(A)   **(B)**   **(C)**

2D domain (Brain 1)   **2D domain (Brain 2)**

(D)   **(E)**

Figure 14. *This figure shows the result of matching the cortical surfaces with one landmark labeled.* (A) *shows the surface of Brain* 1. *It is mapped to Brain* 2 *under conformal parameterization, as shown in* (B). (C) *shows the result of matching using our proposed algorithm.* (D) *and* (E) *show the standard* 2D *parameter domains for Brain* 1 *and Brain* 2, *respectively.*

meshes with 30,000 vertices, Algorithm 1 converges in fewer than 250 iterations on average. The total computational cost, including the initial conformal flattening of the surface meshes, takes on average less than 231 seconds.

9. Conclusion and future work. In this paper, we deal with the problem of surface registration by parameterizing the surface data. Specifically, we developed an algorithm to find parameterizations of the surfaces that are close to conformal which also give a *shape-based*
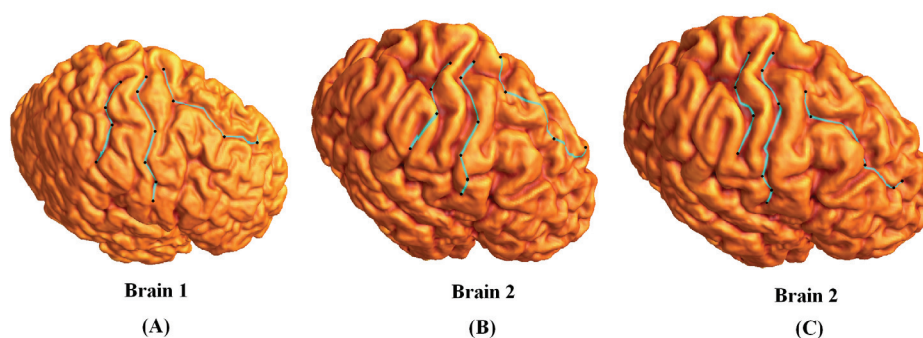
Figure 15. *Illustration of the result of matching the cortical surfaces with several sulcal landmarks.* (A) *shows brain surface* 1. *It is mapped to brain surface* 2 *under the conformal parameterization as shown in* (B). (C) *shows the result of matching under our proposed parameterization.*
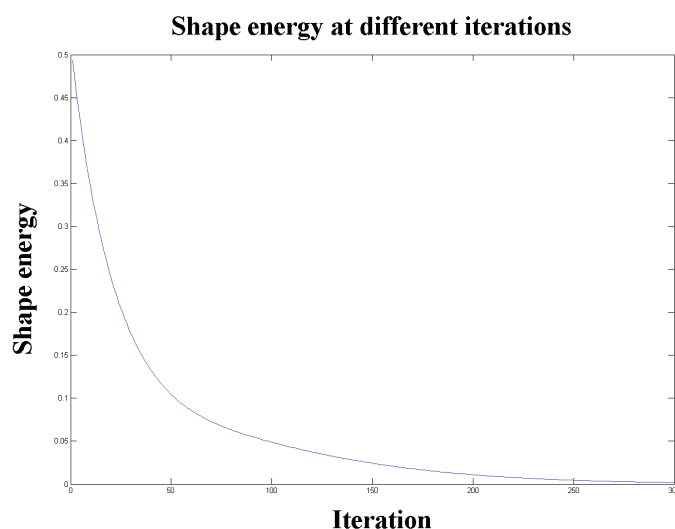

Figure 16. *The shape energy at different iterations.*

correspondence between embedded landmark curves. We propose a variational approach by minimizing a compounded energy that measures the harmonic energy of the parameterizations and the shape dissimilarity between mapped points on the landmark curves. The parameterizations computed are guaranteed to align landmark curves exactly and give a *shape-based* diffeomorphism between them. We tested Algorithm 1 on synthetic surface data to compute the parameterizations of the surfaces that match landmarks using shape-based criteria. We also illustrated the application of our proposed algorithm on real brain cortical surfaces. Experimental results show that Algorithm 1 can effectively compute parameterizations of cortical surfaces that align landmark features consistently with shape correspondence, while preserving the conformality as much as possible. In future work, we plan to apply this algorithm to cortical models from healthy and diseased subjects to build population shape averages.

The enforcement of higher-order shape correspondences may allow subtle but systematic differences in cortical patterning to be detected, for instance, in neurodevelopmental disorders such as Williams syndrome, where the scope of cortical folding anomalies is of great interest but is currently unknown. Another area of interest is to work on better numerical schemes to improve computational efficiency and accuracy.

REFERENCES

[1] A. ALMHDIE, C. LÉGER, M. DERICHE, AND R. LÉDÉE, 3D registration using a new implementation of the ICP algorithm based on a comprehensive lookup matrix: Application to medical imaging, Pattern Recogn. Lett., 28 (2007), pp. 1523–1533.

[2] B. AMBERG, S. ROMDHANI, AND T. VETTER, Optimal step nonrigid ICP algorithms for surface registration, in Proceedings of the IEEE Conference on Computer Vision and Pattern Recognition (CVPR '07), 2007, pp. 1–8.

[3] S. ANGENENT, S. HAKER, R. KIKINIS, AND A. TANNENBAUM, Laplace-Beltrami operator and brain surface flattening, IEEE Trans. Med. Imaging, 18 (1999), pp. 700–711.

[4] S. ANGENENT, S. HAKER, R. KIKINIS, AND A. TANNENBAUM, Nondistorting flattening maps and the 3D visualization of colon CT images, IEEE Trans. Med. Imaging, 19 (2000), pp. 665–671.

[5] M. P. D. CARMO, Differential Geometry of Curves and Surfaces, Prentice-Hall, Englewood Cliffs, NJ, 1976.

[6] S. CHERN, W. CHEN, AND K. LAM, Lectures on Differential Geometry, World Scientific, River Edge, NJ, 1999.

[7] C. DAVATZIKOS AND R. N. BRYAN, Morphometric analysis of cortical sulci using parametric ribbons: A study of the central sulcus, J. Comput. Assist. Tomogr., 26 (2002), pp. 298–307.

[8] H. DRURY, D. V. ESSEN, M. CORBETTA, AND A. SNYDER, Surface-based analyses of the human cerebral cortex, in Brain Warping, Academic Press, San Diego, CA, 1999, pp. 337–363.

[9] S. DURRLEMAN, X. PENNEC, A. TROUVE, P. THOMPSON, AND N. AYACHE, Measuring brain variability via sulcal lines registration: A diffeomorphic approach, in Medical Image Computing and Computer-Assisted Intervention (MICCAI 2007), Lecture Notes in Comput. Sci. 4791, Springer-Verlag, Berlin, Heidelberg, 2007, pp. 675–682.

[10] S. DURRLEMAN, X. PENNEC, A. TROUVE, P. THOMPSON, AND N. AYACHE, Inferring brain variability from diffeomorphic deformations of currents: An integrative approach, Med. Image Anal., 12 (2008), pp. 626–637.

[11] D. C. V. ESSEN, J. W. LEWIS, H. A. DRURY, N. HADJIKHANI, R. B. TOOTELL, M. BAKIRCIOGLU, AND M. I. MILLER, Mapping visual cortex in monkeys and humans using surface-based atlases, Vision Res., 41 (2001), pp. 1359–1378.

[12] B. FISCHL, M. SERENO, R. TOOTELL, AND A. DALE, High-resolution intersubject averaging and a coordinate system for the cortical surface, Human Brain Mapping, 8 (1999), pp. 272–284.

[13] F. GARDINER AND N. LAKIC, Quasiconformal Teichmuller Theory, American Mathematical Society, Providence, RI, 2000.

[14] J. GLAUNÈS, A. TROUVÉ, AND L. YOUNES, Diffeomorphic matching of distributions: A new approach for unlabelled point-sets and sub-manifolds matching, in Proceedings of the IEEE Computer Society Conference on Computer Vision and Pattern Recognition (CVPR), 2004, pp. 712–718.

[15] J. GLAUNÈS, M. VAILLANT, AND M. MILLER, Landmark matching via large deformation diffeomorphisms on the sphere, J. Math. Imaging Vision, 20 (2004), pp. 179–200.

[16] G. L. GOUALHERA, A. M. ARGENTI, M. DUYME, W. F. C. BAARE, H. E. H. POL, D. I. BOOMSMA, A. ZOUAOUI, C. BARILLOT, AND A. C. EVANSA, Statistical sulcal shape comparisons: Application to the detection of genetic encoding of the central sulcus shape, NeuroImage, 11 (2000), pp. 564–574.

[17] X. GU, Y. WANG, T. F. CHAN, P. M. THOMPSON, AND S. T. YAU, Genus zero surface conformal mapping and its application to brain surface mapping, IEEE Trans. Med. Imaging, 23 (2004), pp. 949–958.

[18] X. GU AND S. T. YAU, Global conformal surface parameterization, in Proceedings of the 2003 Eurographics/ACM SIGGRAPH Symposium on Geometry Processing, Aachen, Germany, 2003, pp. 127–137.

[19] S. HAKER, S. ANGENENT, A. TANNENBAUM, R. KIKINIS, G. SAPIRO, AND M. HALLE, Conformal surface parameterization for texture mapping, IEEE Trans. Vis. Comput. Graph., 6 (2000), pp. 181–189.

[20] H. HUANG, S. LI, R. ZHANG, F. MAKEDON, A. SAYKIN, AND J. PEARLMAN, *A novel surface registration algorithm with biomedical modeling applications*, IEEE Trans. Info. Technol. Biomed., 11 (2007), pp. 474–482.

[21] M. K. HURDAL, P. L. BOWERS, K. STEPHENSON, D. W. L. SUMNERS, K. REHM, K. SCHAPER, AND D. A. ROTTENBERG, *Quasi-conformally flat mapping the human cerebellum*, in Medical Image Computing and Computer-Assisted Intervention (MICCAI'99), Lecture Notes in Comput. Sci. 1679, Springer-Verlag, Berlin, Heidelberg, 1999, pp. 279–286.

[22] M. HURDAL AND K. STEPHENSON, *Cortical cartography using the discrete conformal approach of circle packings*, NeuroImage, 23 (2004), pp. S119–S128.

[23] A. JOHNSON AND M. HEBERT, *Surface registration by matching oriented points*, in Proceedings of the International Conference on Recent Advances in 3-D Digital Imaging and Modeling, IEEE Computer Society, Washington, DC, 1997, pp. 121–128.

[24] A. JOSHI, R. LEAHY, P. THOMPSON, AND D. SHATTUCK, *Cortical surface parameterization by p-harmonic energy minimization*, in Proceedings of the IEEE International Symposium on Biomedical Imaging, Arlington, VA, R. Leahy and C. Roux, eds., 2004, pp. 428–431.

[25] L. JU, J. STERN, K. REHM, K. SCHAPER, M. HURDAL, AND D. ROTTENBERG, *Cortical surface flattening using least square conformal mapping with minimal metric distortion*, in Proceedings of the Second IEEE International Symposium on Biomedical Imaging, 2004, pp. 77–80.

[26] J. M. LEE, *Riemannian Manifolds: An Introduction to Curvature*, Springer-Verlag, New York, 1997.

[27] A. LEOW, C. YU, S. LEE, S. HUANG, H. PROTAS, R. NICOLSON, K. HAYASHI, A. TOGA, AND P. THOMPSON, *Brain structural mapping using a novel hybrid implicit/explicit framework based on the level-set method*, NeuroImage, 24 (2005), pp. 910–927.

[28] V. D. LISEIKIN, *Grid Generation Methods*, Springer-Verlag, Berlin, 1999.

[29] L. LUI, Y. WANG, AND T. F. CHAN, *Solving PDEs on manifolds with global conformal parametrization*, in Proceedings of the Third International Workshop on Variational, Geometric, and Level Set Methods in Computer Vision, Lecture Notes in Comput. Sci. 3752, Springer-Verlag, Berlin, Heidelberg, 2005, pp. 307–319.

[30] L. M. LUI, Y. WANG, T. F. CHAN, AND P. THOMPSON, *Automatic landmark tracking and its application to the optimization of brain conformal mapping*, in Proceedings of the IEEE Computer Society Conference on Computer Vision and Pattern Recognition (CVPR), Vol. 2, 2006, pp. 1784–1792.

[31] L. M. LUI, T. W. WONG, W. ZENG, X. GU, P. THOMPSON, T. CHAN, AND S.-T. YAU, *Detecting local shape abnormalities using Yamabe flow and Beltrami coefficients*, Inverse Problems Imaging, to appear.

[32] O. LYTTELTON, M. BOUCHER, S. ROBBINS, AND A. EVANS, *An unbiased iterative group registration template for cortical surface analysis*, NeuroImage, 34 (2007), pp. 1535–1544.

[33] A. A. MICHEL, F. P. FERRIE, AND T. M. PETERS, *An algorithmic overview of surface registration techniques for medical imaging*, Med. Image Anal., 4 (2000), pp. 201–217.

[34] R. PIENAAR, B. FISCHL, V. CAVINESS, N. MAKRIS, AND P. E. GRANT, *A methodology for analyzing curvature in the developing brain from preterm to adult*, Human Brain Imaging, 18 (2008), pp. 42–68.

[35] U. PINKALL AND K. POLTHIER, *Computing discrete minimal surfaces and their conjugates*, Experiment. Math., 2 (1993), pp. 15–36.

[36] Y. SHI, P. THOMPSON, I. DINOV, S. OSHER, AND A. TOGA, *Direct cortical mapping via solving partial differential equations on implicit surfaces*, Med. Image Anal., 11 (2007), pp. 207–223.

[37] H. D. TAGARE, D. O'SHEA, AND D. GROISSER, *Non-rigid shape comparison of plane curves in images*, J. Math. Imaging Vision, 16 (2002), pp. 57–68.

[38] S. R. THIRUVENKADAM, D. GROISSER, AND Y. CHEN, *Non-rigid shape comparison of implicitly-defined curves*, in Proceedings of the Third International Workshop on Variational, Geometric, and Level Set Methods in Computer Vision, Lecture Notes in Comput. Sci. 3752, Springer-Verlag, Berlin, Heidelberg, 2005, pp. 222–234.

[39] P. THOMPSON, K. HAYASHI, E. SOWELL, N. GOGTAY, J. GIEDD, J. RAPOPORT, G. DE ZUBICARAY, A. JANKE, S. ROSE, J. SEMPLE, D. DODDRELL, Y. WANG, T. VAN ERP, T. CANNON, AND A. TOGA, *Mapping cortical change in Alzheimer's disease, brain development, and schizophrenia*, NeuroImage, 23 (2004), pp. S2–S18.

[40] D. TOSUN, M. RETTMANN, AND J. PRINCE, *Mapping techniques for aligning sulci across multiple brains*, Med. Image Anal., 8 (2004), pp. 295–309.

[41] L. WANG, F. BEG, T. RATNANATHER, C. CERITOGLU, L. YOUNES, J. MORRIS, J. CSERNANSKY, AND M. MILLER, *Large deformation diffeomorphism and momentum based hippocampal shape discrimination in dementia of the Alzheimer type*, IEEE Trans. Med. Imaging, 26 (2007), pp. 462–470.

[42] Y. WANG, M.-C. CHIANG, AND P. M. THOMPSON, *Automated surface matching using mutual information applied to Riemann surface structures*, in Medical Image Computing and Computer-Assisted Intervention (MICCAI 2005), Lecture Notes in Comput. Sci. 3750, Springer-Verlag, Berlin, Heidelberg, 2005, pp. 666–674.

[43] Y. WANG, W. DAI, X. GU, T. F. CHAN, S.-T. YAU, A. W. TOGA, AND P. M. THOMPSON, *Teichmüller shape space theory and its application to brain morphometry*, in Medical Image Computing and Computer-Assisted Intervention (MICCAI 2009), Lecture Notes in Comput. Sci. 5762, Springer-Verlag, Berlin, Heidelberg, 2009, pp. 133–140.

[44] Y. WANG, X. GU, T. CHAN, AND P. THOMPSON, *Shape analysis with conformal invariants for multiply connected domains and its application to analyzing brain morphology*, in Proceedings of the IEEE Computer Society Conference on Computer Vision and Pattern Recognition (CVPR), 2009, pp. S39–S41.

[45] Y. WANG, X. GU, K. M. HAYASHI, T. F. CHAN, P. M. THOMPSON, AND S.-T. YAU, *Brain surface parameterization using Riemann surface structure*, in Medical Image Computing and Computer-Assisted Intervention (MICCAI 2005), Lecture Notes in Comput. Sci. 3750, Springer-Verlag, Berlin, Heidelberg, 2005, pp. 657–665.

[46] Y. WANG, X. GU, AND S. YAU, *Surface parameterization using Riemann surface structure*, in Proceedings of the Tenth IEEE International Conference on Computer Vision (ICCV), 2005, pp. 1061–1066.

[47] Y. WANG, L. M. LUI, T. F. CHAN, AND P. M. THOMPSON, *Optimization of brain conformal mapping with landmarks*, in Medical Image Computing and Computer-Assisted Intervention (MICCAI 2005), Lecture Notes in Comput. Sci. 3750, Springer-Verlag, Berlin, Heidelberg, 2005, pp. 675–683.

[48] Y. WANG, L. LUI, X. GU, K. HAYASHI, T. CHAN, A. TOGA, P. THOMPSON, AND S.-T. YAU, *Brain surface conformal parameterization using Riemann surface structure*, IEEE Trans. Med. Imaging, 26 (2007), pp. 853–865.

[49] S. M. YAMANY AND A. A. FARAG, *Free-form surface registration using surface signatures*, in Proceedings of the Seventh IEEE International Conference on Computer Vision (ICCV), Vol. 2, 1999, pp. 1098–1104.

[50] S. YOSHIZAWA, A. BELYAEV, H. YOKOTA, AND H.-P. SEIDEL, *Fast, robust, and faithful methods for detecting crest lines on meshes*, Comput. Aided Geom. Design, 25 (2008), pp. 545–560.

[51] L. YOUNES, *Optimal matching between shapes via elastic deformations*, J. Image Vision, 17 (1999), pp. 381–389.

[52] W. ZENG, L. M. LUI, X. GU, AND S.-T. YAU, *Shape analysis by conformal modules*, Methods Appl. Anal., 15 (2008), pp. 539–556.

[53] J. ZHANG, Y. GE, S. H. ONG, C. K. CHUI, S. H. TEOH, AND C. H. YAN, *Rapid surface registration of 3D volumes using a neural network approach*, Image Vision Comput., 26 (2008), pp. 201–210.